An Analysis of the Hot Jupiter HAT-P-32b and Planetary System of the F-Type Star HAT-P-32

D. A. Mason
University of Durham
(April 10, 2024)

Abstract—We report the observation and analysis of the stellar and planetary characteristics of the HAT-P-32 system. Using aperture photometry, we assess that HAT-P-32 is a late F early G class star with a mass of 1.2 ± 0.2 $M_{\odot}$ and radius of 1.3 ± 0.2 $R_{\odot}$ with an effective temperature of 6170K. We then observe the transit of the exoplanet HAT-P-32b plotting the respective light curve of the flux received from the host star during this period. Our analysis reveals the properties of the planet as a period of 1.4 ± 0.4 days, mass of 2.4 ± 1.4 M_J, radius of 1.8 ± 0.2 R_J and semi-major axis of 0.02 ± 0.01 Au. We further assess that the planet HAT-P-32b has an effective stellar flux $S_{eff} \approx$ 2000 times that of Earth and (amongst other reasons) subsequently does not fall within the habitable zone of HAT-P-32. We go on to discuss the necessary planetary parameters to exist within the habitable zone of the star before addressing the limitations of the study.

Index Terms—Exoplanets, Transit, HAT-P-32, HAT-P-32b, Habitable Zone, Light curve, Hot Jupiter

1 Introduction

Exoplanets exist outside of our solar system, the majority of which are found orbiting a host star. Research into exoplanets is an increasingly popular field of study that unifies a multitude of disciplines in science including astronomy, planetary dynamics physics and astrobiology. This expanding field holds exciting prospects for understanding planetary systems and their development. There is also the capacity to analyse the habitable zones of the host stars and subsequent investigation into the potential of exoplanets' capacities to support carbon-based life, If found, would likely be in a form similar to the chemotrophs on Earth due to the simplicity of the organism and the ability to derive energy from oxidised molecules such as reduced carbon dissolved in water (Westall and Brack, 2018).

1.1 History

Cosmologists have long suspected the existence of planets outside of the solar system, with speculations dating back as far as the 16th century in which Giordano Bruno proposed that distant stars were simply 'other suns with their own planets moving around them'(Kiang, 2017). Despite the longstanding theory, it was only with the development of the radial velocity method in 1992 that proof of exoplanets' existence came about. This method of detection involves observing Doppler shifts in the light spectrum of a star. As a planet orbits its host, it has a gravitational influence which acts on the star with a discrete effect, where the observed velocity respective to Earth can be seen to alter. There is an observable Doppler shift. (Wright, 2018). Such an observation was made by Mayor and Queloz (1995) and was the first proven exoplanet found around a main sequence star. As of 30th March 2024, there have been 5,602 confirmed discoveries and a further 10,157 candidates since the initial 1992 finding (NASA Exoplanet Archive, 2024a). A timeline of all confirmed findings and their respective discovery method is shown in Figure 1.

1.2 Other detection methods:

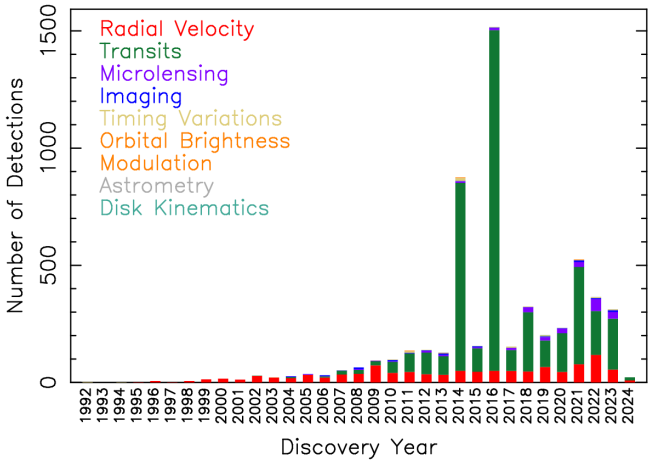

Fig. 1: Timeline illustrating the evolution of exoplanet discovery methods from 1992 to 2024 NASA Exoplanet Archive (2024a)

As shown in Figure 1, since the emergence of the radial velocity method and the first exoplanet discoveries, the field has grown drastically with several other methods of discovery being founded including Microlensing and Imaging. Imaging is the direct observation of photons emitted by an exoplanet. The obstacle to this technique is the omission of the photons emitted by the host star (Wright and Gaudi, 2013). Due to this difficulty, it is not used particularly

frequently and is only credited with the discovery of 68 exoplanets. Gravitational Microlensing, however, is credited with 210 (NASA Exoplanet Archive, 2024a) discoveries. This method works by utilising the effect of the star's gravity which focuses the light of distant sources (Wright and Gaudi, 2013). If a planet is present there is a period where both bodies focus the light toward the observer, causing a 'blip' of brightness. The timings of this method cannot be predicted so astronomers observe the sky for any changes in the brightness of stars and the lensing potential. This method has also been used to detect 'rogue planets' - free-floating planets in space that can cause their short-lasting microlensing events.

1.3 The Transit Method

The most notable of the detection methods was the transit method. First used in 1999, this technique accounts for 74.4% of all exoplanet discoveries to date. (NASA Exoplanet Archive, 2024a) There are obvious peaks in 2014 and 2016 when NASA used the Kepler Space Telescope (KST) for their first and second planet-hunting missions. This telescope and its purpose have since been replaced by the Transiting Exoplanet Survey Satellite (TESS), another NASA-run project targeting an area 400 times greater than that observed by the KST. This project is responsible for 7,125 of the current exoplanet candidates (NASA Exoplanet Archive, 2024c). As the name suggests, the transit method involves monitoring the brightness of the host star as the planet passes in front of it. During this period, the planet blocks a portion of the star's emitted light, making it appear dimmer. As seen in Figure 2 , a light curve of the observed brightness of the star can be plotted during this process. Light curves allow scientists to calculate useful information regarding the properties of both the star and the planet. A pivotal advancement allowing for these calculations and analysis was the development of the Mandel and Agol (2002) Model.

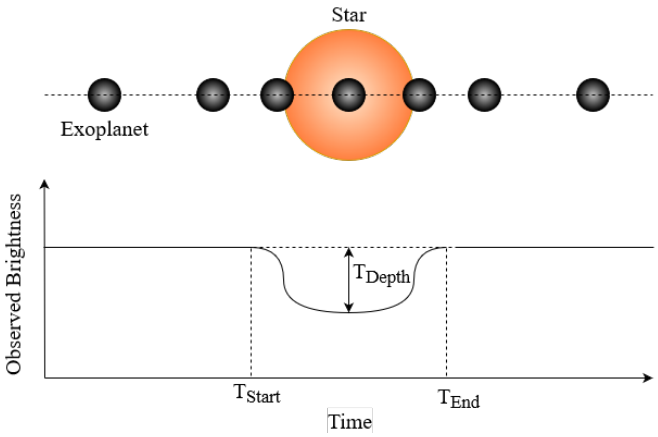

Fig. 2: A visualisation of an exoplanet transiting its host star with a corresponding example light curve where T_{Start} and T_{End} are the beginning and end of the transit respectively and T_{Depth} represents the observed reduction in brightness of the host star at the center of the transit.

This report exploits the transit method in an observation of the star HAT-P-32 with the ultimate aim of calculating the planet's key characteristics and its relation with its Host Star. We further aim to assess the habitable zone of HAT-P-32.

2 Observations and Data Reduction

2.1 Observation specifications

In the course of the investigation, HAT-P-32 was observed on two occasions (a full observation table is shown in Appendix A). The primary observation, conducted on January 14th, was focused on the collection of data regarding the transit itself where the approximate start time was supplied by the Exoplanet Transit Database (Poddaný et al., 2010). During this session, conditions were optimal with clear skies and wind speeds of 12mph contributing to an average full width at half maximum value of 2.24 arcseconds. Taking advantage of this, 966 images were taken in the V band filter with exposure times of 30 seconds. These choices offered optimal data collection parameters as we had complete coverage of the transit with ample data points that had enough light to be useful but had not over-saturated the CCD. The V band was chosen purposefully to reap the benefits of the atmospheric transparency at this wavelength thereby minimising the light distortion and improving the potential for precise data analysis (Condon and Ransom, 2016).

On January 15th, the secondary observation was undertaken where a total of 12 images were collected in the colour filters B, V, R and C which allowed for the construction of the deep-field mosaic shown in Figure 3. These observation sessions were conducted at the Durham University undergraduate observatories predominantly utilising the 'Far-East-20 telescope'. This telescope possesses a 50cm aperture and focal ratio of 10, offering a balance between a large field of view and high-resolution imagery. It is further equipped with a 10-micron GM3000 mount allowing for precise and stable tracking of targets. The telescope also boasts a Moravian C4-1600 camera, beneficial for our data acquisition as the detectors were sensitive enough to differentiate the subtle signal variations received from HAT-P-32 during the transit phase of the exoplanet.

2.2 Data processing

Before analysing the images, standard preprocessing techniques such as dark frame subtraction and flat field correction were applied to each image. This ensured a correction for any variation in the pixel sensitivity of the CCD as well as the subtraction of the inherent electronic noise of the sensor.

To effectively analyse the images, we carried out aperture photometry on each. This involved counting the flux within a given area (aperture) surrounding the target star and

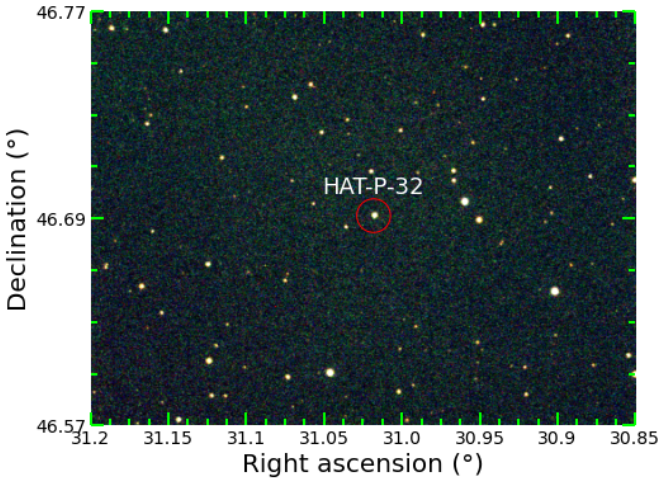

Fig. 3: A Deepfield colour image of the Star HAT-P-32 captured January 15th 2024

subtracting the average background noise (given by the defined counts within the inner and outer range of a defined annulus). Then, using the known magnitudes of surrounding stars, a calibration can be determined. This was carried out by using the zeropoint formulae as shown in equations 1 and 2, knowing this calibration allows for the calculation of the magnitude of the target star.

$$\mathrm{ZP} = m_{\mathrm{std}} - m_{\mathrm{inst,\,std}} \tag{1}$$

$$m_{\mathrm{actual}} = ZP - m_{\mathrm{inst,\,Obj}} \tag{2}$$

Where ZP is the zeropoint value, m_{std} is the known magnitude of the calibration star as provided by Zacharias et al. (2013), $m_{\mathrm{inst,\,std}}$ is the instrumental magnitude of the calibration star and similarly $m_{\mathrm{inst,\,target}}$ is the instrumental magnitude of the target star and finally m_{actual} is the calibrated magnitude of the target star.

As a result, a crucial step was deciding on the aperture size as this determined the measured signal of the target star and subsequently had a great effect on the signal-to-noise ratio (S/N). In this investigation having an optimal S/N was vital as the method relied on an observable change in the star's brightness, this change was fractional when compared to the actual brightness of the star and as such it was important to be able to distinguish the transit from background noise. Thus calculating the optimal aperture size was necessary. To address this, a range of aperture sizes between 0.8 and 12 arcseconds was evaluated by creating a script that returned the magnitude and respective error of HAT-P-32 for all 966 images using the same procedure as described above, where 2 calibration stars were used. This data, for every aperture size, was recorded and subsequently produced Figure 4. This graph was produced by cleaning each dataset by removing any rows that contained anomalous data points especially those with inflated errors on the magnitude outside of the set threshold of 0.02 magnitudes. Then histograms of the errors and respective Gaussian fits which produced the average error and standard deviation for each aperture size plotted. From this, we evaluate an aperture size of 5 seconds to be optimal as it minimises the error on the calculated magnitude to a value of 0.0042 magnitudes.

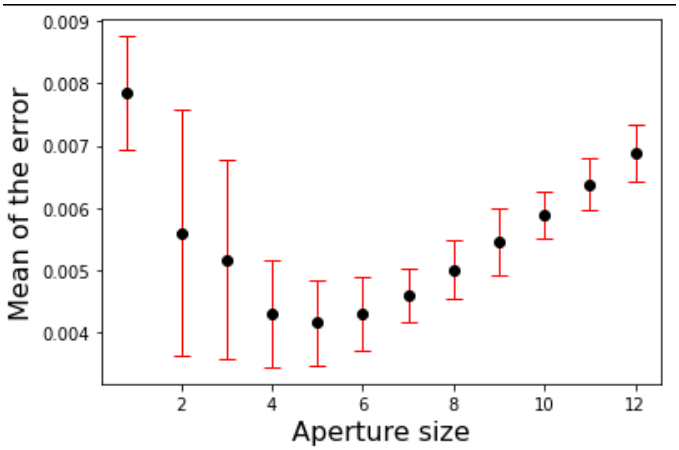

Fig. 4: A plot of the relationship between the aperture size and corresponding average error on the magnitude of HAT-P-32

3 Analysis

3.1 Stellar Parameters

Having observed the star we were able to calculate a key informative property, its colour. To achieve this, the magnitudes of HAT-P-32 in both the B band and V band were calculated using the same method described in section2.2. We used stacked mosaic images where the calibration magnitudes are again provided by Zacharias et al. (2013). These magnitudes and their respective errors give us a colour value range in the commonly used B-V colour index which we used to infer a stellar class using the work of Pecaut and Mamajek (2013), where the assumption is made that the HAT-P-32 is a main sequence star. Furthermore, with the B-V value we can calculate a range on the effective temperature of the star using Equation (3), an approximation provided by Ballesteros (2012) derived by fitting observed stellar temperatures to theoretical black body radiation curves. Following this, we calculated the luminosity of the star using the stellar distance as provided by NASA Exoplanet Archive (2024b) and the previously calculated apparent magnitude.

$$T_{\mathrm{eff}} = 4600\left(\frac{1}{0.92(B-V)+1.7} + \frac{1}{0.92(B-V)+0.62}\right) \tag{3}$$

Knowing these characteristics allowed for the calculation of the stellar mass and radius with Equations (4) and (5) below:

$$\left(\frac{M_*}{M_\odot}\right)^{3.5} = \left(\frac{L_*}{L_\odot}\right) \tag{4}$$

$$\frac{R_*}{R_\odot} = \sqrt{\frac{\frac{L_*}{L_\odot}}{(\frac{T_*}{T_\odot})^4}} \tag{5}$$

3.2 Model Fitting

To extract useful information from the primary observation a light curve similar to the one shown in Figure 2 must be produced and a model fitted to it. To achieve this we made use of the Python library `PyTransit` (Parviainen, 2015). This is a specialised library purposed specifically for analysing the light curve of transiting planets. Being optimised for computational speed when exploring parameter spaces and possessing a user-friendly interface proved to be pivotal in the analysis stage of our investigation.

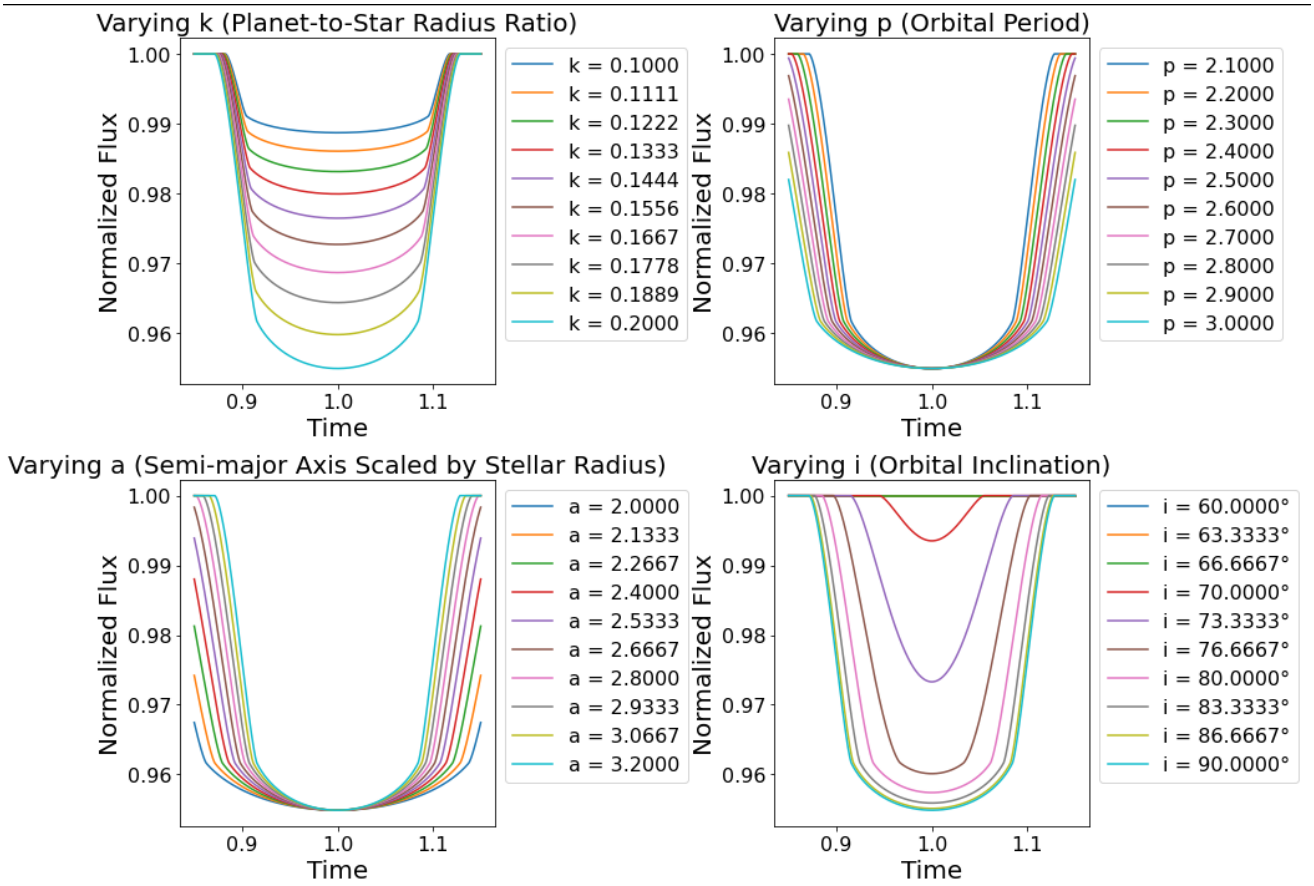

Fig. 5: A demonstration of how varied values of key parameters (k, p, a and i) impact a Quadratic Limb darkening model (QLDM)

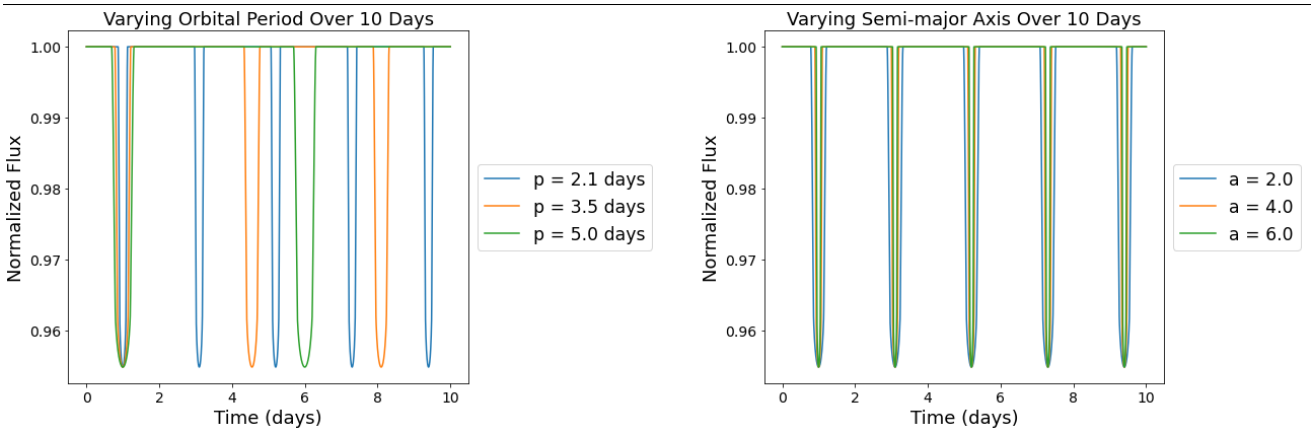

Fig. 6: A demonstration of the effects of a varied orbital period and semi-major axis on the QLDM over an extended time frame

We elected to use the `QuadtraticModel` within `PyTransit` in our analysis, this was because it is an extension of the well-founded model provided by Mandel and Agol (2002). The only difference in the models is their approach to describing the limb darkening of the star. As implied, the quadratic model used assumes a quadratic function that describes how the brightness of a star lessens towards its edges. This approach offers a better fit to the data than a linear limb darkening coefficient.

Before attempting to model the transit data of HAT-P-32b, we conducted an exploratory analysis of the key parameters and their influence on a surrogate light curve which can be seen in Figure 5. These included the planet-to-star radius ratio (k), the orbital period (P), the semi-major axis (a) and the orbital inclination (i). The limb darkening coefficients were not investigated as these were taken as known constants the values relative to HAT-P-32 taken as [0.405,0.284] using our defined stellar parameters and comparison tables in the work of Claret and Bloemen (2011). Useful conclusions could be inferred from an analysis of Figures 5 and 6, such as an increased planet-to-star radius ratio resulting in a deeper transit. This means physically that larger planets block more of the star's observed light resulting in a more noticeable reduction of brightness. The model indicates a planet twice the radius of a hypothetical base planet with k value of 0.1 would increase the depth by over 3%. The graph also displayed a symmetry suggesting the deepest point at the centre of the curve relates to when the exoplanet is directly aligned with the host star. As would be expected, a longer orbital period resulted in a longer transit duration presented as a wider light curve. Over an extended duration demonstrated in Figure 6 an observed decrease in the frequency of transits also became apparent for increased orbital periods. Conversely, an increased semi-major axis demonstrated a decrease in the transit width this is a result of transit geometry whereas the semi-major axis increases, the angular size of the star decreases, meaning it takes less time to pass across, hence a shorter transit. Unlike the period, the semi-major axis does not affect the frequency of the transit. Alterations made to the orbital inclination showed a change in the shape of the transit as well as having considerable effects on the transit depth, with inclinations closest to 90°maximising the observable difference in brightness. This is because when the planet transits directly across the centre of the star, relative to the observer, it maximises the light that it blocks from its host.

Following this parameter exploration, we endeavoured to plot the best-fit model to our data of HAT-P-32. To achieve this we used the Markov Chain Monte Carlo (MCMC) method to construct a parameter probability distribution. This was a necessity due to the many potential combinations of parameter values which could fit the observational data. The MCMC was an ideal tool to utilise as it allowed for the characterisation of a distribution without knowing all of the mathematical properties. The algorithm achieved this by starting at given arbitrary values and iteratively sampling values out of the distribution (van Ravenzwaaij et al., 2016). This process involves a chain where each sample is dependent only on the previous step. As the process progresses the parameter values converge and eventually the most likely combination of the values of k, t_0 p a and i are found. Where the parameters are defined as they were in Figure 5 and t_0 is the mid-point of the transit.

In our instance, an initial optimisation was carried out using `scipy.optimize` (Virtanen et al., 2020) which began with an initial guess of parameter values and iteratively improved upon them by minimising the negative likelihood of observing data under the model. These best-fit parameters were used as a starting point for the MCMC sampling where a script was written using the Python library `emcee` (Foreman-Mackey et al., 2013), a specially designed library designed for efficient Bayesian MCMC sampling. In our analysis, we utilised an ensemble sampler where 30 separate walkers were used to explore the parameter space with 100,000 samples each. The choice of having 30 walkers increased the coverage of the space without exceptional computational expense. As well as this, the increased number of chains contributed to a faster convergence as demonstrated in the trace plot Figure 7b. To analyse the results we first disregarded the initial 5,000 samples as this ensured the walkers had fully converged to the target distribution. The remaining samples were considered a posterior distribution meaning they were assumed to accurately represent the target distribution. These samples were averaged with uncertainties quoted as two standard deviations corresponding to a certainty level of 95%. These optimal values are quoted in Table 1.

TABLE 1: Comparison of the most likely parameters and the mean parameters with errors, as determined using MCMC for k, t_0, p, a, and i

Parameters	Units	Most Likely Values	Mean Values and Errors
k	N/A	0.1356	0.136 ± 0.002
t_0	hours	1.987	1.99 ± 0.02
p	hours	24.846	34 ± 19
a	R_*	3.07	4.2 ± 2.3
i	rads	1.55	1.57 ± 0.07

Figure 7a showcases a corner plot constructed from the posterior samples generated by the MCMC analysis. The histograms displayed along the diagonal of the graph can be used to make judgments on the confidence of the estimates, where the shape of the plot gives immediate visual feedback, where sharp peaks suggest greater confidence than the broader distributions, as we can confidently consider the value of parameters k, t_0 and i. Less so the values of p and a.

Underneath the diagonal, the relationship between each pair of parameters can be observed where deviations from a circular shape can infer covariances. Therefore there is a particular interest in the relationship between the orbital period and semi-major axis. The plot shows a positive covariance between the parameters shown by the positive linear shape

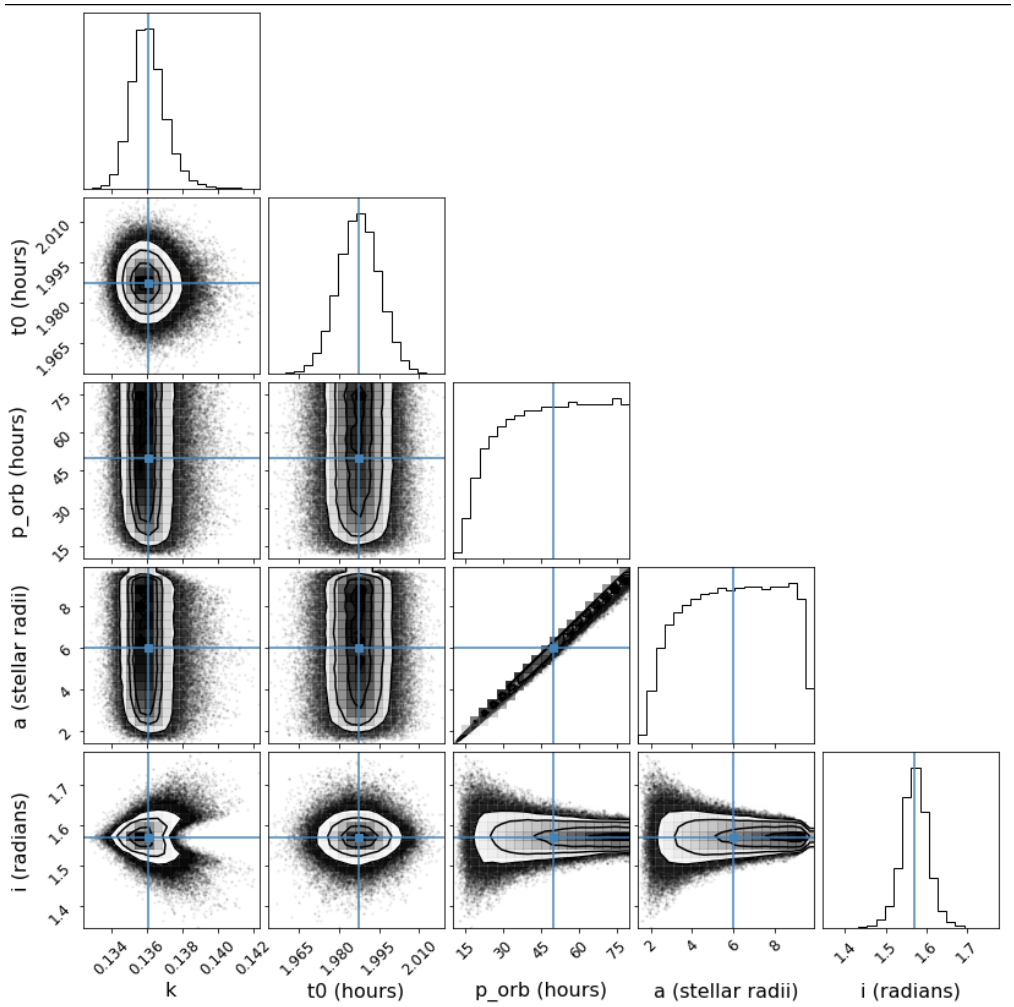

(a) Contour plots displaying the covariance between pairs of parameters (k, t_0, p, a, i)

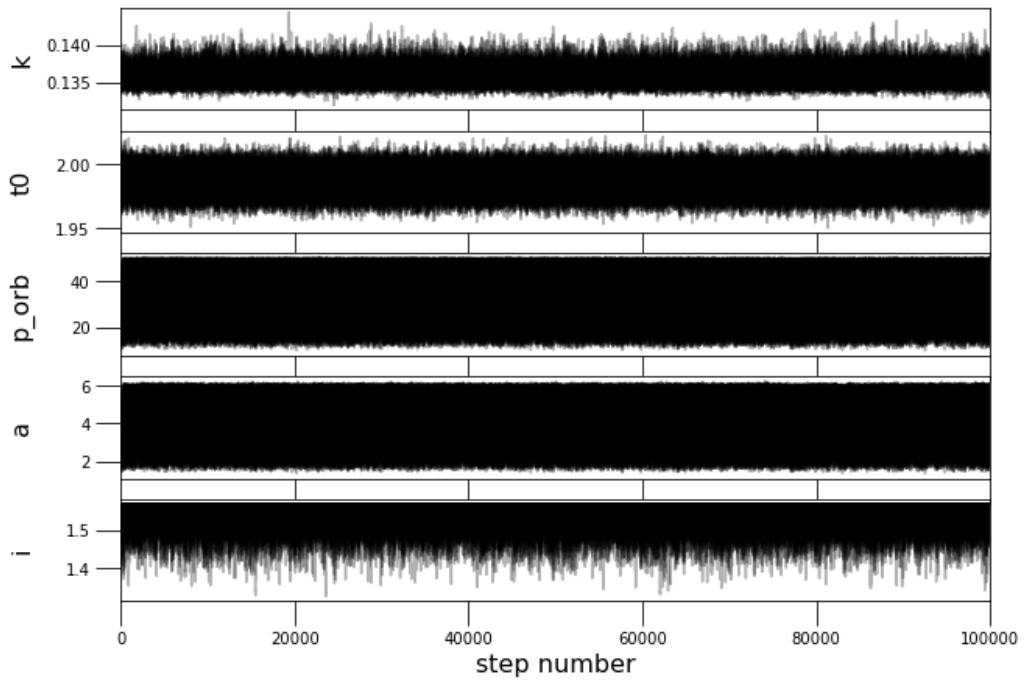

(b) Trace Plots of MCMC Walkers for the HAT-P-32b Parameters demonstrating the convergence of the MCMC sampling 100,000 steps for parameters k, t_0, p, a, and i.

Fig. 7: MCMC Analysis of Exoplanet HAT-P-32b

in Figure 7a this makes sense following Kepler's third law (6) which states that the square of the Orbital period is proportional to the cube of the semi-major axis. This also offered some explanation for the proportionally large error margins on both of these parameters compared to the errors on k, t_0 and i which were all under 2.3% as there is little certainty in predicting the value of one without accurate prior knowledge of the other. There are also the near-circular plots between k and t_0 as well as i and t_0 showing independence in these pairs of variables.

$$P^2 = \frac{4\pi^2}{G(M_1 + M_2)}a^3 \tag{6}$$

Having calculated the specific optimal parameters for HAT-P-32 to use in the Quadratic limb darkening model, Figure 8 was produced. Where the plotted violet line is the fitted model using the parameter means and the dashed black line was plotted using the maximum likelihood of the parameters as defined in Table 1. These plots are nearly identical, this suggests a multitude of local minima that allows for many combinations of the covariant parameters overall meaning the MCMC may not be able to accurately predict these values. The pale red region represents the range between the minimum and maximum flux values obtained from all of the simulated outputs. The orange region, however, represents the range of flux values where the parameters p and a are constrained to result in planetary mass distribution between 0.36 and 11.8M_J when used in Kepler's third law (6), these value is taken as threshold masses of the definition of a Hot Jupiter as given by Winn et al. (2010). This was achieved by bootstrapping the error distributions assuming Gaussian errors. Overall demonstrating where the model predicts the flux values could reasonably fall following these constraints.

A visual investigation reveals that both models fit the data well with 79.5% of the normalised residuals having values less than 3. This idea is further reinforced by the χ^2_{red} value for the models being close to 1.

3.3 Planetary Parameters

Using our mass distribution we were then able to calculate a mean planetary mass and standard deviation, however, as a result of the previously established covariance between p and a, determining an accurate value of the planetary mass using the transit method proves difficult. Ordinarily, the radial velocity method proves a better option as the orbital period is observed directly and therefore a more accurate

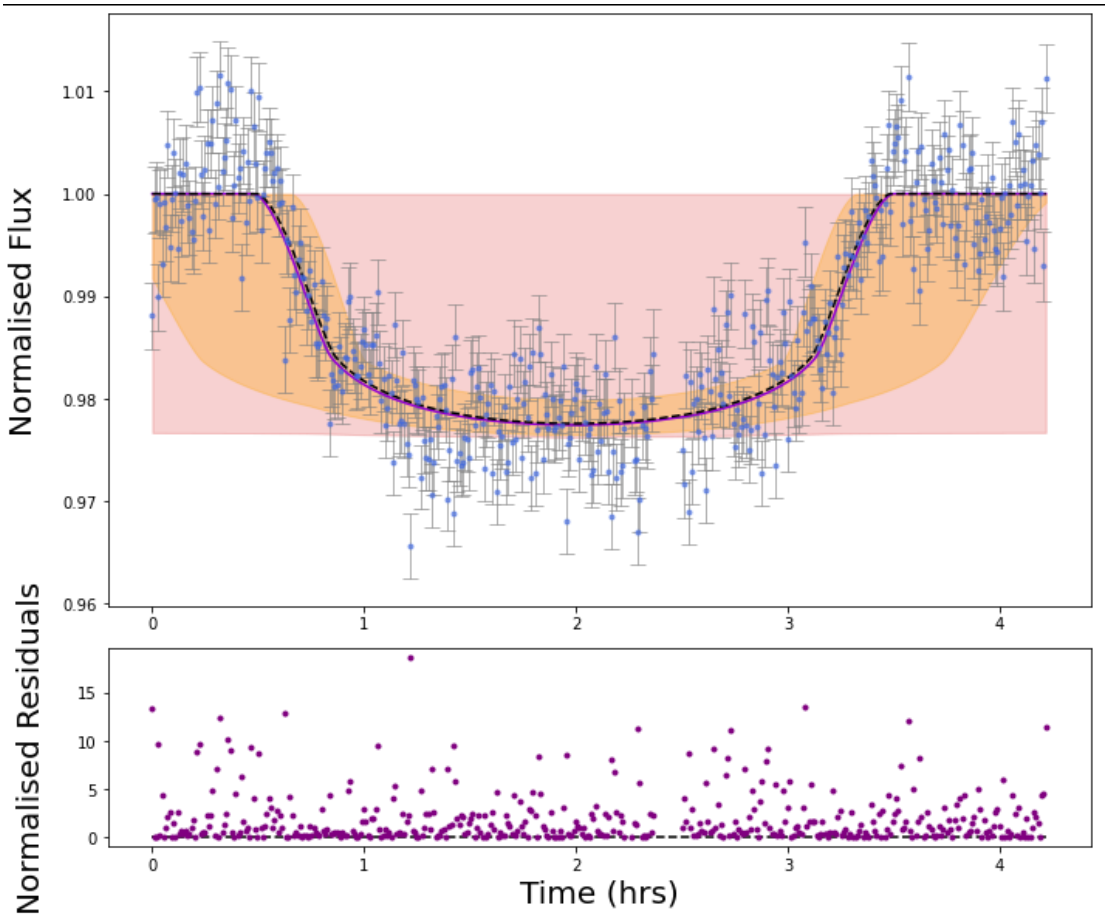

Fig. 8: A fitted light curve depicting the transit of HAT-P-32 and corresponding residuals of the best-fit model as well as a plot of the residuals

value of both p and a can be calculated, for reference these parameters and the corresponding planetary mass using both methods are presented in Table 2 below, where the errors of this work are quoted at a 95% certainty level (It can be noted at this point that the planet does indeed meet the criteria of a Hot Jupiter as given by Winn et al. (2010) , where it must have a mass between 0.36 and 11.8 M_J and an orbital period between 1.3 and 111 days).

TABLE 2

Parameter	Units	Values and Errors	
		This Work	**Hartman et al. (2011)**
Orbital Period	$days$	1.4 ± 0.8	2.150008 ± 0.000001
Semi-Major axis	Au	0.022 ± 0.012	0.0343 ± 0.0004
Planetary Mass	M_J	2.4 ± 2.8	0.860 ± 0.164

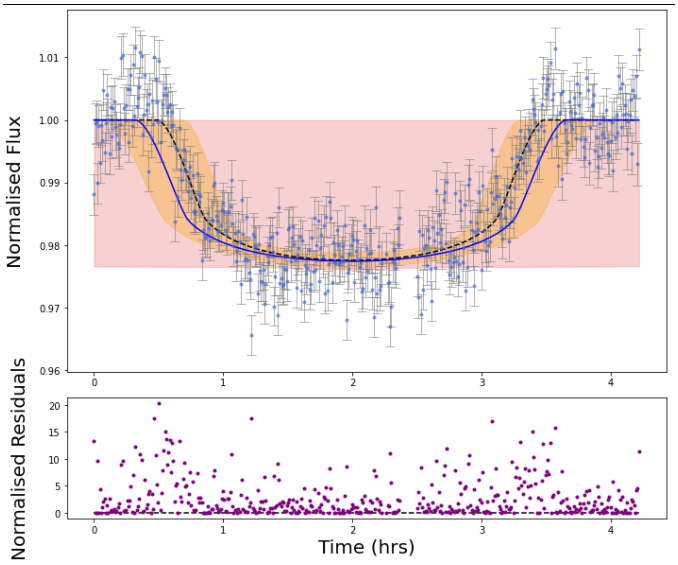

Fig. 9: An experimental model of the light curve incorporating the parameters p and a as provided by Hartman et al. (2011) in Table 2

In Figure 9 these parameter values are exchanged in the plotting of the model, where the new curve is shown in blue with the previous most likely parameters curve remaining the same. The effect, as could be predicted after our parameter exploration in Figure 5 is a wider transit. This effect, however, is not so drastic that the model exceeds the threshold of our defined error region. Despite this, the new model does not fit the data points with the same level of accuracy. This model results in less than 70% of the normalised residuals being at a value below 3. However, due to the inaccuracies and uncertainty in the parameter definitions for a and p from the shortcomings of the MCMC method, the necessary parameters needed for calculating the planetary mass cannot be trusted from our findings. As a result, we will proceed to speculate on the planetary conditions utilising the values given by Hartman et al. (2011) having used the radial velocity method.

3.4 Planetary Conditions

To calculate the effective temperature of HAT-P-32b we used Equation (7) assuming a bond albedo (A) similar to that of Jupiter due to the similarities in being gas giants. We, therefore, used a value of 0.503 ± 0.012 (Li et al., 2018)

$$T_p = T_* \sqrt{\frac{R_*}{2a_p}} [1 - A]^{\frac{1}{4}} \tag{7}$$

Following this, using the assumed mass of 0.860 M_J (Hartman et al., 2011) we calculated the potential atmospheric conditions of HAT-P-32b, for instance, the escape velocity of the planet is calculated to have a value of 42 ± 2 Kms^{-1} using equation 8. This of course determines the gaseous composition of the planet's atmosphere by affecting which particles can escape the gravitational pull. This means that the atmospheric composition is determined by the thermal energy a gas molecule has and whether this exceeds the escape velocity. We can use the Maxwell-Boltzmann distribution (10) (Hernandez, 2017) to display this. It was assumed that due to the tails of the distribution if $V_{rms} > \frac{V_{esc}}{10}$ (8)(9) then the gas is likely to evaporate from the atmosphere.

$$V_{esc} = \sqrt{\frac{2GM_p}{R_p}} \tag{8}$$

$$V_{rms} = \sqrt{\frac{3k_B T_{eff}}{m}} \tag{9}$$

$$f(v) = 4\pi \left(\frac{m}{2\pi k_B T}\right)^{\frac{3}{2}} v^2 e^{-\frac{mv^2}{2k_B T}} \tag{10}$$

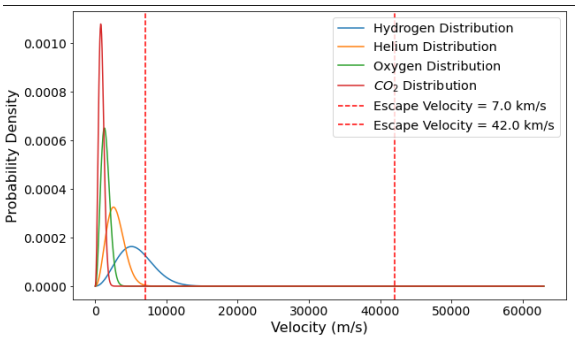

Fig. 10: The Maxwell-Boltzmann distribution of gases at an equilibrium temperature of 1563K

In terms of composition, the planet is likely to be predominantly light gases such as hydrogen and helium. This is due to its vast size but comparatively small density meaning an unlikelihood of rocky or metallic substances (Swift et al., 2011). In the plots in Figure 10 , we observe that the tails of the helium and a sizeable region of the hydrogen distributions exceed the criteria established meaning the planet is likely losing mass as these gases evaporate into

space. As such it is likely that over an extended period, due to photoevaporation, the planet will lose a considerable amount of its mass. Czesla, S. et al. (2022) suggest the planet may have already lost over half the mass it had at birth and will continue to diminish until the end of its host star's life cycle.

Due to the planet's proximity to the star, it experiences incredible tidal forces calculated to be in the order of $10^{27}N$ approximately 2×10^8 times greater than the tidal forces experienced by Earth from the sun. Subsequently, the planet may experience significant tidal heating as the internal friction from the gravitational deformation generates heat. Furthermore, the planet is likely to be tidally locked, meaning a temperature gradient might have formed across the planet resulting in extreme wind speeds (Heng and Showman, 2015) potentially exceeding the speed of sound in air (Fortney et al., 2021). The face of the planet closest to the star would experience continuous heating and therefore may also potentially experience strong storm systems.

$$\mid \vec{F} \mid = \frac{4GM_*M_pR_p}{a_p^3} \tag{11}$$

3.5 The Habitable zone of HAT-P-32

The habitable zone (HZ) of a star is the region in which it would be possible for the surface of a planet to sustain liquid water (Kasting et al., 2013). In the classification of the HZ, we assume we are dealing with Earth-like planets with $CO_2/H_2O/N_2$ atmospheres orbiting a main sequence star (Kasting et al., 1993). The HZ is dependent on several factors, in its most conservative form it is calculated as the difference between the point of a 'runaway greenhouse' effect and a 'Maximum greenhouse'. The runaway greenhouse effect is when a planet's atmosphere is unable to prevent excess buildup of heat to a point where any present water escapes the atmosphere of the planet as vapour(Nakajima et al., 1992), and the Maximum greenhouse effect is where the planet has an atmosphere rich enough in CO_2 that it can trap enough heat that it is prevented from freezing over. Further than this conservative estimate, there is an optimistic estimate for the range of the habitable zone between what is known as a 'recent Venus' threshold, which is an extension of the greenhouse runaway, and the 'Early Mars' Threshold. The recent Venus threshold is the ultimate point before a planet becomes inhospitable and the 'Early Mars' threshold is based on the idea that though Mars was frozen over, earlier in its existence it may have retained liquid water due to a thicker atmosphere.

These boundaries can be defined by an effective stellar flux (S_{eff}) and subsequently a distance given by Equations (13)and (14) where the coefficients are provided by Ramirez (2018) (Schwieterman et al., 2019). Using these equations we calculated HAT-P-32b to have a $S_{eff} \approx 2000$ times that of earth.

$$T^* = T_{eff} - 5780 \tag{12}$$

$$S_{eff} = S_{sun} + aT^* + bT^{*2} + cT^{*3} + dT^{*4} \tag{13}$$

$$d = \sqrt{\frac{L_*}{S_{eff}}} \tag{14}$$

With this information, we can plot the relationship between the distance to the habitable zone and the star's effective temperature. Knowing this, we can prioritise searching for Earth-like planets in the HZ by implementing constraints on the orbital characteristics of the planet.

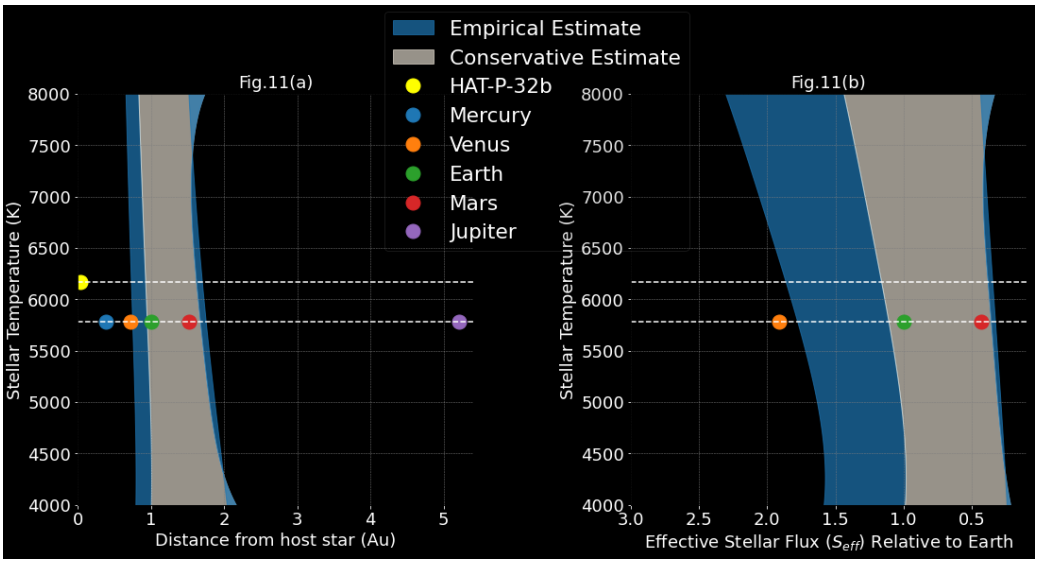

Fig. 11: (a): Comparison of the planetary systems surrounding HAT-P-32 and the sun.
(b): A closer inspection of the habitable zone in the effective stellar flux relative to Earth for different effective stellar temperatures. (Note, the size of the markers used distorts the distance from the star, in actuality, HAT-P-32b is over 11 $\times$ closer to their respective stars than mercury.)

TABLE 3: The final results table for the parameters associated with the HAT-P-32 system with errors taken at a 95% confidence range

Parameter	Units	Value	Error	Reference
Stellar Parameters				
RA	hours : Minutes : Seconds	02 : 04 : 10.24	N/A	(Poddaný et al., 2010)
DEC	Degrees : Minutes : Seconds	+46 : 41 : 16.8	N/A	(Poddaný et al., 2010)
B Magnitude	mag	11.75	0.04	This work
V Magnitude	mag	11.21	0.07	This work
Spectral Type	N/A	F8	F4 - G3	This work
Mass	$M_\odot$	1.2	0.2	This work
Radius	$R_\odot$	1.3	0.2	This work
Luminosity	$L_\odot$	2.35	0.09	This work
Density	$g\ cm^{-3}$	4.1	0.2	This work
Effective temperature	K	6170	450	This work
Metallicity	[Fe/H]	-0.04	0.080	(Nortmann et al., 2016)
Age	Gyr	2.70	0.80	(Bonomo et al., 2017)
Planetary Parameters				
Orbital Period	days	1.4	0.8	This work
Semi-major axis	Au	0.022	0.012	This work
Mass	M_J	2.4	1.4	This work
Radius	R_J	1.8	0.3	This work
Planetary Parameters Using Radial Velocity				
Radial Velocity Amplitude	$m\ s^{-1}$	122.8	23.2	(Hartman et al., 2011)
Semi-major axis	Au	0.0343	0.0004	(Hartman et al., 2011)
Orbital period	Hours	2.15.0008	0.000001	(Hartman et al., 2011)
Mass	M_J	0.860	0.164	(Hartman et al., 2011)
Equilibrium Temperature	K	1560	190	This work
Escape velocity	Kms^{-1}	42	2	This work
Transit Parameters				
Transit Duration	hours	2.99	0.133	This work
Semi-major axis	R_*	4.15	1.14	This work
Inclination of the Orbit	Degrees	90.0	4.0	This work
Planet to Star radius Ratio	R_P/R_*	0.1356	0.0009	This work
Transit centre	hours	1.99	0.02	This work

4 Discussion and Conclusion

This report has presented an analysis of the properties of a hot Jupiter and its host star as well as the relationship between them making use of the transit method of detection. We have further speculated on the habitable region of the star concluding that HAT-P-32b lies far too close to its host to be habitable.

Our analysis estimated the mass and radius of the planet to be (2.4 ± 2.8 M_J) and (1.8 ± 0.2 R_J) respectively, these values align well with the previous definition of a hot Jupiter (Winn et al., 2010) despite the considerable error margins.

From our analysis, we can agree with the evaluation from Hartman et al. (2011) that HAT-P-32b is a highly inflated Hot Jupiter, where the planet is seen to have a radius significantly larger than expected by planetary evolution models such as those presented by Fortney et al. (2007). We also acknowledge that our calculated radius presents HAT-P32b as one of the largest known exoplanets.

Due to limitations of the transit method concerning observing some planetary parameters, we notice obvious differences in the mass when compared to peers' work. We accredit this discrepancy to the covariance between the semi-major axis and orbital period resulting in limited accuracy in the knowledge of these parameters perpetuating into the calculation of the mass of the planet using 6 where both p and a are heavily weighted being to the power 2 and 3 respectively. To mitigate this future works could use the Exoplanet Transit Database (Poddaný et al., 2010) to align their observations with two successive observable transits and use the time difference as a first guess in the MCMC. This could further enable them to set more precise constraints for the priors of the orbital period. Had we done this, we may have avoided the local minima in the MCMC and could hold a greater deal of certainty in the values of p, a and subsequently the mass of HAT-P-32b.

Alternatively, future researchers, with access to a sensitive spectrograph, could expand our methodology and attempt Doppler spectroscopy, using the periodicity of the spectral shifts to calculate an accurate orbital period (Eggenberger and Udry, 2010). With the use of both methodologies in tandem the results for the high uncertainty parameters may diverge less significantly from other works.

Other limitations in our observations included the nature of conducting a singular observation which meant that any reduction in random atmospheric noise that multiple observations may have offered was not possible. Furthermore, we relied on the photometry of the star to calculate its colour when ideally we would have performed spectroscopy, this

would have given a greater knowledge of the properties of the star, including a more accurate temperature that could have been calculated using Wein's law. Spectroscopy may have also offered insight into the stellar composition by relating the perceived spectral lines to specific elements.

In future research, it could be enlightening to calculate the mass loss rate of the planet and observe the gaseous tail left by evaporating hydrogen and helium. This could offer insight as to why the nearest hot Jupiter to its host so far observed has been limited to an orbital distance of 0.014 Au (Czesla, S. et al., 2022). This line of inquiry may offer suggestions as to how proximity to the host star influences planetary evolution. This could be because a closer proximity to the star could further increase the irradiation of the planet and therefore the equilibrium temperature, potentially increasing the rate of mass loss. It may also prove effective to use data acquired from specially tasked space telescopes such as ARIEL which will perform spectroscopic surveys of the atmospheres of transiting planets (Pascale et al., 2018).

Other avenues for future observations of the system could include microlensing the calculated habitable zone in hopes of observing terrestrial planets. This would prove more effective for trying to observe an Earth-like planet in the habitable zone than the transit method as this technique is more suited to the high semi-major axis and smaller radii associated with this kind of observation.

To conclude, this investigation into the Hot Jupiter HAT-P-32b and its host star HAT-P-32 offers a practical methodology in the detection and analysis of a large and close orbiting exoplanet using the transit method. We summarise key parameters associated with both the star and the planet as well as the transit properties themselves. The report offers an effective approach to measuring the radius, inclination and transit duration relating to HAT-P-32b but discloses difficulty in measuring other planetary parameters such as the orbital period and semi-major axis. We offer an explanation for this and future recommendations to mitigate the effects.

5 Acknowledgments

This research has made use of both the telescopes and analysis software namely GAIA (Draper et al., 2021) and DS9 (Joye and Mandel, 2003) which were generously provided by Durham University.
The author would also like to give thanks to their research partner Alex Nicholson for their contributions in data acquisition and analysis.

References

Ballesteros, F. J. (2012). New insights into black bodies. *EPL (Europhysics Letters)*, 97(3):34008. 10.1209/0295-5075/97/34008.

Bonomo, A. S., Desidera, S., Benatti, S., Borsa, F., Crespi, S., Damasso, M., Lanza, A. F., Sozzetti, A., Lodato, G., Marzari, F., and et al. (2017). The gaps programme with harps-n at tng. *Astronomy & Astrophysics*, 602. 10.1051/0004-6361/201629882.

Claret, A. and Bloemen, S. (2011). Gravity and limb-darkening coefficients for thekepler, corot,spitzer,uvby,ubvrijhk, and sloan photometric systems. *Astronomy amp; Astrophysics*, 529. 10.1051/0004-6361/201116451.

Condon, J. J. and Ransom, S. M. (2016). Essential radio astronomy. *Essential radio astronomy*. 10.1515/9781400881161.

Czesla, S., Lampón, M., Sanz-Forcada, J., García Muñoz, A., López-Puertas, M., Nortmann, L., Yan, D., Nagel, E., Yan, F., Schmitt, J. H. M. M., Aceituno, J., Amado, P. J., Caballero, J. A., Casasayas-Barris, N., Henning, Th., Khalafinejad, S., Molaverdikhani, K., Montes, D., Pallé, E., Reiners, A., Schneider, P. C., Ribas, I., Quirrenbach, A., Zapatero Osorio, M. R., and Zechmeister, M. (2022). H and hei absorption in hat-p-32 b observed with carmenes - detection of roche lobe overflow and mass loss. *AA*, 657:A6. 10.1051/0004-6361/202039919.

Draper, P. W., Gray, N., Berry, D. S., and Taylor, M. (2021).

Eggenberger, A. and Udry, S. (2010). Detection and characterization of extrasolar planets through doppler spectroscopy. *EAS Publications Series*, 41:27–75. 10.1051/eas/1041002.

et al, K. A. (2019). Qatar exoplanet survey: Qatar-8b, 9b, and 10b—a hot saturn and two hot jupiters. *The Astronomical Journal*, 157(6):224. 10.3847/1538-3881/ab19bc.

Foreman-Mackey, D., Hogg, D. W., Lang, D., and Goodman, J. (2013). emcee: The mcmc hammer. *PASP*, 125:306–312. 10.1086/670067.

Fortney, J. J., Dawson, R. I., and Komacek, T. D. (2021). Hot jupiters: Origins, structure, atmospheres. *Journal of Geophysical Research: Planets*, 126(3). 10.1029/2020je006629.

Fortney, J. J., Marley, M. S., and Barnes, J. W. (2007). Planetary radii across five orders of magnitude in mass and stellar insolation: Application to transits. *The Astrophysical Journal*, 659(2):1661. 10.1086/512120.

Hartman, J. D., Bakos, G. Á., Torres, G., Latham, D. W., Kovács, G., Béky, B., Quinn, S. N., Mazeh, T., Shporer, A., Marcy, G. W., Howard, A. W., Fischer, D. A., Johnson, J. A., Esquerdo, G. A., Noyes, R. W., Sasselov, D. D., Stefanik, R. P., Fernandez, J. M., Szklenár, T., Lázár, J., Papp, I., and Sári, P. (2011). HAT-P-32b and HAT-P-33b: Two Highly Inflated Hot Jupiters Transiting High-jitter Stars. , 742(1):59. 10.1088/0004-637X/742/1/59.

Heng, K. and Showman, A. P. (2015). Atmospheric dynamics of hot exoplanets. *Annual Review of Earth and Planetary Sciences*, 43(Volume 43, 2015):509–540. https://doi.org/10.1146/annurev-earth-060614-105146.

Hernandez, H. (2017). Standard maxwell-boltzmann distribution: definition and properties. *ForsChem Research Reports*, 2:2017–2.

Joye, W. A. and Mandel, E. (2003). New Features of SAOImage DS9. In Payne, H. E., Jedrzejewski, R. I., and Hook, R. N., editors, *Astronomical Data Analysis Software and Systems XII*, volume 295 of *Astronomical Society of the Pacific Conference Series*.

Kasting, J. F., Kopparapu, R., Ramirez, R. M., and Harman, C. E. (2013). Remote life-detection criteria, habitable zone boundaries, and the frequency of earth-like planets around m and late k stars. *Proceedings of the National Academy of Sciences*, 111(35). 10.1073/pnas.1309107110.

Kasting, J. F., Whitmire, D. P., and Reynolds, R. T. (1993). Habitable zones around main sequence stars. *Icarus*, 101(1):108–128. https://doi.org/10.1006/icar.1993.1010.

Kiang, N. Y. (2017). Biosignatures of exoplanets. *Capeia*, 2017.

Li, L., Jiang, X., West, R. A., Gierasch, P. J., Perez-Hoyos, S., Sanchez-Lavega, A., Fletcher, L. N., Fortney, J. J., Knowles, B., Porco, C. C., and et al. (2018). Less absorbed solar energy and more internal heat for jupiter. *Nature Communications*, 9(1). 10.1038/s41467-018-06107-2.

Mandel and Agol (2002). *Analytic Light Curves for Planetary Transit Searches*. The American Astronomical Society. 10.1086/345520.

Mayor, M. and Queloz, D. (1995). A jupiter-mass companion to a solar-type star. *Nature*, 378(6555). 10.1038/378355a0.

Nakajima, S., Hayashi, Y.-Y., and Abe, Y. (1992). A study on the "runaway greenhouse effect" with a one-dimensional radiative–convective equilibrium model. *Journal of Atmospheric Sciences*, 49(23):2256 – 2266. 10.1175/1520-0469(1992)049¡2256:ASOTGE¿2.0.CO;2.

NASA Exoplanet Archive (2024a). Pre-generated exoplanet plots.

NASA Exoplanet Archive (2024b). Tess project candidates.

NASA Exoplanet Archive (2024c). Transiting exoplanet survey satelite.

Nortmann, L., Pallé, E., Murgas, F., Dreizler, S., Iro, N., and Cabrera-Lavers, A. (2016). The gtc exoplanet transit spectroscopy survey. *Astronomy & Astrophysics*, 594. 10.1051/0004-6361/201527323.

Parviainen, H. (2015). PYTRANSIT: fast and easy exoplanet transit modelling in PYTHON. , 450(3). 10.1093/mnras/stv894.

Pascale, E., Eccleston, P., and Tinetti, G. (2018). The ariel space mission. In *2018 5th IEEE International Workshop on Metrology for AeroSpace (MetroAeroSpace)*, pages 31–34. 10.1109/MetroAeroSpace.2018.8453588.

Pecaut, M. J. and Mamajek, E. E. (2013). Intrinsic colors, temperatures, and bolometric corrections of pre-main-sequence stars. *The Astrophysical Journal Supplement Series*, 208(1):9. 10.1088/0067-0049/208/1/9.

Poddaný, S., Brát, L., and Pejcha, O. (2010). Exoplanet transit database. reduction and processing of the photometric data of exoplanet transits. *New Astronomy*, 15(3).

Ramirez, R. (2018). A more comprehensive habitable zone for finding life on other planets. *Geosciences*, 8(8):280. 10.3390/geosciences8080280.

Schwieterman, E. W., Reinhard, C. T., Olson, S. L., Harman, C. E., and Lyons, T. W. (2019). A limited habitable zone for complex life. *The Astrophysical Journal*, 878(1):19. 10.3847/1538-4357/ab1d52.

Swift, D. C., Eggert, J. H., Hicks, D. G., Hamel, S., Caspersen, K., Schwegler, E., Collins, G. W., Nettelmann, N., and Ackland, G. J. (2011). Mass–radius relationships for exoplanets. *The Astrophysical Journal*, 744(1):59. 10.1088/0004-637X/744/1/59.

van Ravenzwaaij, D., Cassey, P., and Brown, S. D. (2016). A simple introduction to markov chain monte–carlo sampling. *Psychonomic Bulletin amp; Review*, 25(1). 10.3758/s13423-016-1015-8.

Virtanen, P., Gommers, R., Oliphant, T. E., Haberland, M., Reddy, T., Cournapeau, D., Burovski, E., Peterson, P., Weckesser, W., Bright, J., van der Walt, S. J., Brett, M., Wilson, J., Millman, K. J., Mayorov, N., Nelson, A. R. J., Jones, E., Kern, R., Larson, E., Carey, C. J., Polat, İ., Feng, Y., Moore, E. W., VanderPlas, J., Laxalde, D., Perktold, J., Cimrman, R., Henriksen, I., Quintero, E. A., Harris, C. R., Archibald, A. M., Ribeiro, A. H., Pedregosa, F., van Mulbregt, P., and SciPy 1.0 Contributors (2020). SciPy 1.0: Fundamental Algorithms for Scientific Computing in Python. *Nature Methods*, 17:261–272. 10.1038/s41592-019-0686-2.

Westall, F. and Brack, A. (2018). The importance of water for life. *Space Science Reviews*, 214(2). 10.1007/s11214-018-0476-7.

Winn, J. N., Fabrycky, D., Albrecht, S., and Johnson, J. A. (2010). Hot stars with hot jupiters have high obliquities. *The Astrophysical Journal*, 718(2):L145–L149. 10.1088/2041-8205/718/2/l145.

Wright, J. T. (2018). *Radial Velocities as an Exoplanet Discovery Method*. Springer International Publishing. 10.1007/978-3-319-55333-7$_4$.

Wright, J. T. and Gaudi, B. S. (2013). Exoplanet detection methods. *Planets, Stars and Stellar Systems*. 10.1007/978-94-007-5606-9$_1$0.

Zacharias, N., Finch, C. T., Girard, T. M., Henden, A., Bartlett, J. L., Monet, D. G., and Zacharias, M. I. (2013). The fourth us naval observatory ccd astrograph catalog (ucac4). *The Astronomical Journal*, 145(2). 10.1088/0004-6256/145/2/44.

APPENDIX A
OBSERVATION LOG

TABLE 4: Observing log

Date	Telescope	Object	Colour Filter	Image count	Exposure time	Notes
13/01/24	Draco	XO-5b	C	60	180	A test observation to familiarise ourselves with the technology and software
14/01/24	Far-east-20	HAT-P-32b	V	966	30.0	Optimal conditions, minimal cloud cover and winds of 12mph
15/01/24	West-14	HAT-P-32b	C, R, B, V	12	4.0	Optimal conditions, minimal cloud cover and winds of 9mph
11/02/24	Far-east-20	Qatar 9b	C	347	60	Predominantly optimal conditions, passing cloud cover in the early stages of observing
11/02/24	Far-east-20	Qatar 9b	R, B, V	12	120	Predominantly optimal conditions, passing cloud cover in the early stages of observing

APPENDIX B
QATAR 9B

A similar study was conducted on the planetary system of the star Qatar 9. The plotted light curve and respective results table are displayed below:

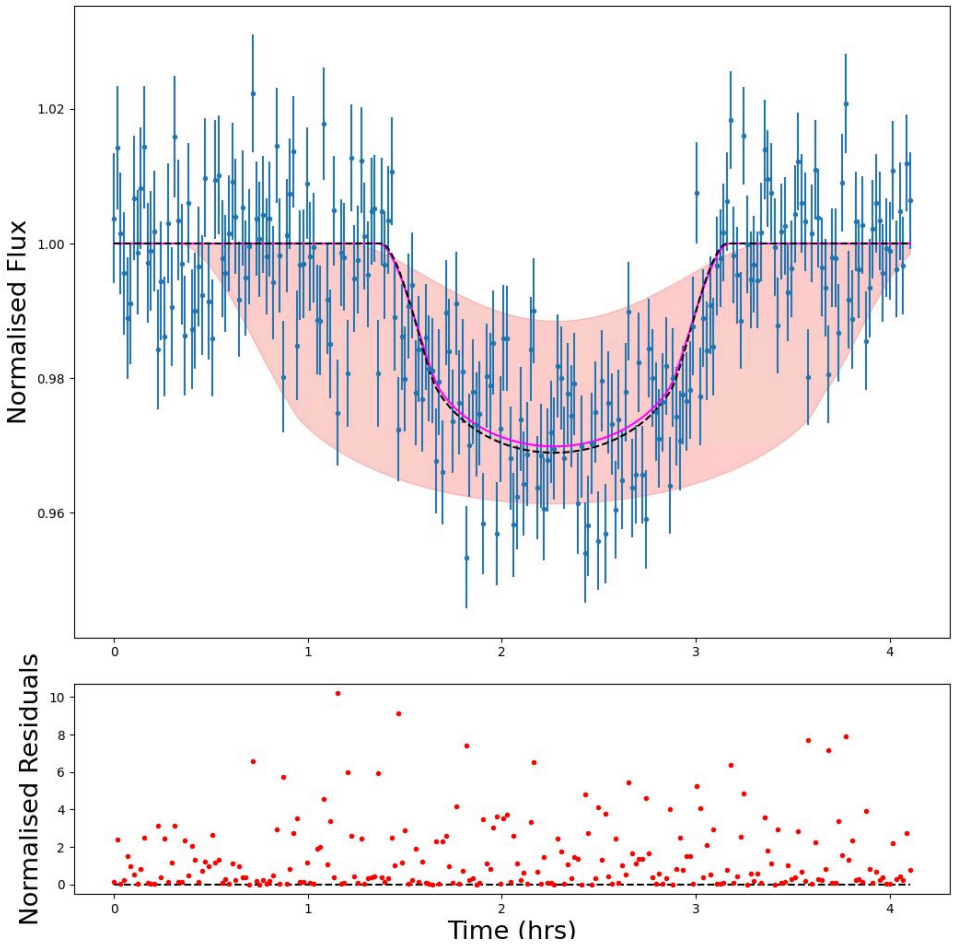

Fig. 12: Enter Caption

TABLE 5: Stellar and Planetary Parameters for the Qatar-9 System with errors at a 68% confidence level

Parameter	Units	Value	Error	Reference
		Stellar Parameters		
RA	hours : Minutes : Seconds	10 : 42 : 59.83	N/A	Poddaný et al. (2010)
DEC	Degrees : Minutes : Seconds	+60 : 57 : 50.83	N/A	Poddaný et al. (2010)
B - V	N/A	1.3	0.1	This work
T_{eff}	K	4200	200	This Work
Spectral Class	N/A	K6V	K5-K8	This Work
L	$L_{\odot}$	0.14	0.02	This work
Mass	$M_{\odot}$	0.57	0.02	This work
Metallicity	[Fe/H]	0.25	0.08	et al (2019)
Radius	$R_{\odot}$	0.696	0.008	et al (2019)
		Planetary Parameters		
Radius	R_{Jup}	1.1	0.3	This work
Orbital Period (T)	hrs	45	2	This work
Semi Major Axis (a_p)	Au	0.02	0.01	This work
Mass	M_{Jup}	0.8	0.5	This work
Density	gcm^{-3}	1.43	0.20	et al (2019)
Equilibrium Temperature	K	1000	200	This work
		Transit parameter		
Inclination	Degrees	88	3	This work
Transit Center (t_0)	hrs	2.27	0.02	This work
Semi-Major axis	$R_{\odot}$	6.2	3.1	This work
Planet to star radius ratio	$R_P/R_{\odot}$	0.155	0.004	This work

APPENDIX C
LAY SUMMARY

An exoplanet is a planet outside of our solar system. We can detect and analyse planets like these where doing so can offer insight into the diversity of planets throughout the universe. Using the Far-East-20 telescope available at Durham University we assess such a particular planet labelled as HAT-P-32b. We can conduct an analysis of this planet by observing the varied observed brightness of its host star (HAT-P-32). This change in brightness reveals some important relationships between the star and planet such as the ratio between the two radii, the distance between the two objects and the time it takes for the planet to orbit the star. Our work calculates these values as 0.136, 0.022 Au and 1.4 days respectively where Au is the average distance between the sun and Earth.

When combined with the calculated stellar radius (1.3 $\times$ that of the sun) we can see we are investigating an incredibly large planet that orbits its star incredibly quickly at a very close proximity. We further investigate the stellar and planetary environments assessing the effective temperature of the star as 5900°C, approximately 400 degrees hotter than that of the sun. The planetary temperature is calculated to be 1290°C with expected extreme weather in the form of extreme winds and storms. Overall we evaluate the planet to likely be comprised mainly of hydrogen and helium, however, we suggest it is likely losing considerable mass in the form of these gases as they evaporate out of the atmosphere. This could form a tail of gas to follow the planet as it orbits, similar in appearance to the tail of a comet. We have rejected the possibility that any liquid water could exist on the planet as it exists far beyond the respective habitable zone of its star as such it is unlikely to find life on HAT-P-32b.

APPENDIX D
GENERATIVE AI STATEMENT

Generative AI was used only with the aid of formatting in the LaTeX environment